Yuan, X., Huppert, K., Braun, J., Shen, X., Liu-Zeng, J., Guerit, L., Wolf, S., Zhang, J., Jolivet, M. (2022): Propagating uplift controls on high-elevation, low-relief landscape formation in the southeast Tibetan Plateau. - Geology, 50, 1, 60-65.

https://doi.org/10.1130/G49022.1

Propagating uplift controls on high-elevation, low-relief landscape formation in Southeast Tibetan Plateau

X. P. Yuan[1,2], K. L. Huppert[2], J. Braun[2], X. Shen[2,3], J. Liu-Zeng[4], L. Guerit[5], S. G. Wolf[6], J. F. Zhang[1], M. Jolivet[5]

[1]School of Earth Sciences, China University of Geosciences, 430074 Wuhan, China

[2]Helmholtz Centre Potsdam, German Research Centre for Geosciences, 14473 Potsdam, Germany

[3]National Institute of Natural Hazards, Ministry of Emergency Management of China, 10085 Beijing, China

[4]Institute of Surface Earth System Science, Tianjin University, 300072 Tianjin, China

[5]University of Rennes, CNRS, Géosciences Rennes, UMR 6118, 35000 Rennes, France

[6]Department of Earth Science, University of Bergen, N-5020 Bergen, Norway

ABSTRACT

High-elevation, low-relief surfaces are widespread in many mountain belts. However, the origin of these surfaces has long been debated. In particular, the Southeast (SE) Tibetan Plateau has extensive low-relief surfaces perched above deep valleys and in the headwaters of three of the world's largest rivers (Salween, Mekong and Yangtze). Various geologic data and geodynamic models show that many mountain belts grow first to a certain height and then laterally in an outward propagation sequence. By translating this information into a kinematic propagating uplift function in a landscape evolution model, we propose that the high-elevation, low-relief surfaces in the SE Tibetan Plateau are simply a consequence of mountain growth and do not require a special process to form. The propagating uplift forms an elongated river network geometry with broad high-elevation, low-relief headwaters and interfluves that persist for tens of millions of years, consistent with the observed geochronology. We suggest that the low-relief interfluves can be long-lived because they are lack of drainage network to keep pace with rapid

incision of the large mainstem rivers. The propagating uplift also produces spatial and temporal exhumation patterns and river profile morphologies that match observations. Our modeling therefore reconciles geomorphic observations with geodynamic models of uplift of the SE Tibetan Plateau, and provides a simple mechanism to explain low-relief surfaces observed in several mountain belts on Earth.

INTRODUCTION

High-elevation, low-relief surfaces are ubiquitous in many mountain belts (e.g., Epis and Chapin, 1975; Kennan et al., 1997; Babault et al., 2005; van der Beek et al., 2009). They are often interpreted to be remnant surfaces of paleo-landscapes and are thus widely used as geomorphic markers to constrain tectonic uplift and landscape evolution (Clark et al., 2006). However, the origin of high-elevation, low-relief surfaces remains highly disputed (e.g., Clark et al., 2006; Liu-Zeng et al., 2008; Yang et al., 2015; Whipple et al., 2017; Bosch et al., 2018; Fox et al., 2020), with previous studies mainly proposing that they either represent a relict pre-uplift low-relief surface, uplifted and eroded by a wave of upstream incision instigated by an increase in rock uplift (Clark et al., 2006; Whipple et al., 2017), or that they formed *in-situ* by tectonic shortening and consequent drainage reorganization (Yang et al., 2015). This debate exists especially in the SE Tibetan Plateau where the low-relief surfaces are widely observed (Fig. 1A).

Three of the world's largest rivers (Salween, Mekong and Yangtze) run from the central Tibetan Plateau across the SE plateau margin (Fig. 1B). High-elevation, low-relief surfaces at elevations 4-6 km above sea level and perched 2-3 km above deep adjacent valleys occupy the headwaters and interfluves of the Three Rivers (Fig. 1B; Clark et al., 2006). Thermochronologic data suggest that rapid incision has been focused within these valleys, with accelerated incision starting at >10–20 Ma (Clark et al., 2005; Ouimet et al., 2010; Tian et al., 2014; Liu-Zeng et al., 2018). In contrast, the low-relief surfaces in the headwaters and interfluves have experienced little erosion during the Cenozoic (Clark et al., 2006), with thermochronologic ages mainly at ~50 Ma (Li et al., 2019). The long-term coexistence of deep valleys and low-relief surfaces raises fundamental questions about (i) the factors controlling the formation of extensive low-relief surfaces, and (ii) the survival of the low-relief surfaces above deep valleys.

Synthesized structural analyses (Wang et al., 2014; Li et al., 2015) and thermochronologic ages (Li et al., 2019) show a younging trend from the central plateau to the SE margin, suggesting that the Tibetan Plateau may have progressively grown southeastward from the central plateau since the Eocene. This uplift pattern is consistent with various geodynamic models and geologic data, which show that many mountain belts grow first to a certain height and then expand laterally in an outward propagation sequence characterized by successive marginal uplift (e.g., Jammes and Huismans, 2012; Wolf et al., 2021).

By translating this information into a simple kinematic uplift function and using a landscape evolution model of long-term fluvial erosion and sediment transport (Yuan et al., 2019; Data Repository Text DR1.1), we investigate whether the propagating uplift is responsible for generating the observed low-relief surfaces.

FORMATION OF BROAD HIGH-ELEVATION, LOW-RELIEF SURFACES

Our models start from an initially random surface with ≤100 m of relief, run for 50 Myr, and shorten uniformly NW-SE and non-uniformly SW-NE (Text DR1.2). In addition to this horizontal deformation, the modeled landscape is subject to a propagating wave of 0.23 mm/yr vertical uplift (Text DR1.3; Fig. 2A) to simulate the outward-propagating growth of the plateau, implied by the thermochronologic and structural data (Wang et al., 2014; Li et al., 2019). Uplift rates at a given point on the landscape are initially zero, gradually increase to 0.23 mm/yr with passage of the propagating uplift wave, then gradually reduce back to zero.

Our simulation shows that propagating uplift promotes the progressive formation of elongated, NE-SW-spanning river basins (Fig. 2A). The initial propagating uplift forms narrow, parallel drainages on the front slope of the propagating margin, and the elongated drainage basins extend downstream during forward propagating of the uplift. The headwaters and interfluves of rivers are characterized by high-elevation, low-relief surfaces (Fig. 2A and 2C). Our results reproduce the observed co-planarity of these low-relief surfaces (Figs. 1D-F and 2D), their height 2-3-km above adjacent valleys (Fig. 2E), as well as their progressive decrease in elevation from NW to SE across the plateau margin (Whipple et al., 2017). This consistency between modeled and observed topography supports our hypothesis that propagating uplift plays a key role in generating high-elevation, low-relief surfaces on the SE Tibetan Plateau. Regardless of the specific erosion and deposition parameters used (Fig. DR5), we show that the propagating uplift controls the first-order erosional dynamic of landscape evolution.

SPATIAL AND TEMPORAL EXHUMATION PATTERNS

In the deep valleys of our simulated mainstem rivers (black dots V1−V4 and curves in Fig. 3A-B), exhumation proceeds initially at a slow rate, accelerates, and then decreases after the uplift wave has passed (V3, V4), consistent with the cooling and exhumation pattern recorded by low-temperature thermochronologic data (e.g., Liu-Zeng et al., 2018; Li et al., 2019). The timing of accelerated exhumation in the mainstem valleys is spatially variable and propagates downstream (Fig. 3A-B), e.g., initiating at ~34 Ma (V4), ~25 Ma (V3), ~20 Ma (V2), and ~12 Ma (V1). This temporal pattern is also consistent with compiled thermochronologic ages showing a younging trend from the central plateau (32−34ºN) to the SE margin (~27ºN) along the mainstem rivers (Li et al., 2019).

Normalized channel steepness k_{sn} (Wobus et al., 2006) is widely used to investigate spatial exhumation patterns and is defined as

$$k_{sn} = SA^{m/n}, \quad (1)$$

where S is the channel slope, A is the drainage area, and m/n is the concavity of the river profile, taken to be 0.4 (Fig. DR2). Our modeling shows that k_{sn} is low in the headwaters (Fig. 2B) and increases downstream in the mainstem rivers, reaching a peak value at the plateau margin, as observed on the SE Tibetan Plateau (Fig. 1B).

Upstream channel reaches in our model erode slowly at long-term rate (e.g., ~650 m/50 Myr = 0.013 mm/yr; slope of the orange curve in Fig. 3B) and short-term rate (0.01–0.015 mm/yr; Fig. 2D) matching observed erosion rates inferred from low-temperature thermochronology (0.01–0.02 mm/yr; Clark et al., 2006) and millennial basin-averaged cosmogenic ^{10}Be erosion rates (0.013–0.024 mm/yr; Henck et al., 2011). Dividing the predicted 2.2 km exhumation of the major river valley (V2; dashed curve in Fig. 3B) by the ~20 Ma onset of accelerated exhumation yields an average erosion rate of 0.11 mm/yr, which is within the range of exhumation rates (~0.1–0.3 mm/yr) from the Miocene to present (20–0 Ma) inferred from thermochronologic data (Liu-Zeng et al., 2018). In contrast, the low-relief interfluves in our model have low long-term erosion rates (500 m/~25 Myr = ~0.02 mm/yr; slope of the cyan curve in Fig. 3B) matching erosion rates inferred from thermochronologic ages of late Miocene remnant surfaces (~0.02 mm/yr; Clark et al., 2005; 2006) and consistent with millennial erosion rates derived from cosmogenic nuclide exposure ages (0.015–0.022 mm/yr; Ouimet et al., 2005; Clark et al., 2006).

The low-relief surfaces erode approximately ten times more slowly than the mainstem valleys and persist relatively unchanged because they lack sufficient drainage area to generate the incision rates necessary to keep pace with rapid incision of the mainstem rivers (Fig. 2A-B). This discrepancy in erosion rates arises because of the unusually elongated river network geometry produced by propagating plateau uplift, with large mainstem rivers fed predominantly by small tributaries along their length. Long, parallel mainstem rivers erode rapidly in response to this uplift while their short, drainage-area starved tributaries fail to keep pace. This unique river network morphology provides an explanation for the persistence of high-elevation, low-relief surfaces and the deep entrenchment of their adjacent mainstem rivers.

RIVER PROFILE MORPHOLOGY

Rivers adjust their slopes in response to changes in uplift, so their morphology records transient landscape evolution. We use plots of elevation versus an upstream integral of drainage area, χ (Perron and Royden, 2013), to quantitatively compare modeled and observed river profiles (Text DR2). The slope of channel elevation with respect to χ is k_{sn}. The χ-elevation plots of the Three Rivers are convex (Fig. 1C), with a higher average k_{sn}= 66 $m^{0.8}$ downstream (<3558±380 m in elevation) and a lower average k_{sn}= 22 $m^{0.8}$ in the upstream headwaters. This change in steepness does not correlate with spatial variations in lithology (Yang et al., 2015) or mean annual precipitation (Figs. 1D-F and DR1).

We model two end-member cases: propagating vs. uniform uplift. The former case is supported by previous studies (Clark et al., 2000; Schoenbohm et al., 2006), while the latter provides a null hypothesis against which to test the propagating uplift model. The propagating uplift can explain changes in steepness (Fig. 3C), and the erodibility K_f of 1.2×10^{-6} $m^{0.2}$/yr provides the best fit between modeled and observed χ-elevation plots (Fig. DR4). We model the latter case of a uniform increase in rock uplift to reach the same final elevation h_f (Equation DR3) from the initial elevation h_i of random ≤100-m white noise, i.e., the rock uplift rate is $U = (h_f - h_i)/50$ Myr. Within the range of possible K_f, river profiles under uniform uplift either span too great an elevation range or grade to nearly uniform steepness along their lengths, dissimilar to the observed fluvial profiles (Figs. 3F and DR7).

Considering both the propagating and uniform uplift models using the same erodibility (K_f = 1.2×10^{-6} $m^{0.2}$/yr) for comparison, results show that uniform uplift can preserve the relict low-relief surfaces in upstream headwaters (Figs. 3D and DR8A-B), corroborating the findings of Whipple et al. (2017), but cannot form deep, narrow mainstem valleys with low-relief interfluves in their middle and lower reaches (Sinclair, 2017). This is because, under uniform uplift, low-relief interfluves are eventually dissected by a wave of upstream-propagating river incision (Fig. DR8C). Furthermore, the modeled timing of accelerated exhumation along the mainstem rivers shows old ages downstream (~35 Ma, V1−V2; Fig. 3E) and younger ages upstream (~10 Ma, V4), inconsistent with the observed trend of thermochronologic ages (Li et al., 2019).

It has alternately been hypothesized that high-elevation, low-relief surfaces may be actively forming and evolving on the SE Tibetan Plateau due to drainage-area reorganization wrought by horizontal tectonic shortening (Yang et al., 2015). While this mechanism may play some role in promoting the development of low-relief surfaces, our modeling shows that such surfaces can form even without dramatic drainage area exchange via discrete river capture events (Fig. 2C). The high-elevation, low-relief surfaces that form in our models do experience some drainage-area loss and gain via progressive drainage divide migration (Movie DR1). However, because drainage area exchange occurs gradually at the earlier stage, it does not significantly modify the remnant low-relief topography, nor does it generate nascent low-relief surfaces *in-situ*. We further run a model without horizontal tectonic deformation, the high-elevation, low-relief surfaces can still form, and the modeled χ-elevation plot also fits the observed one (Fig. DR9).

CONCLUSIONS

Our work brings a new explanation for the genesis of high-elevation, low-relief surfaces, and shows that these surfaces in the SE Tibetan Plateau are simply a consequence of mountain growth. Using shortening and uplift parameters (Text DR1) for the specific example of southeastern Tibet, we show that propagating uplift of mountain growth produces broad high-elevation, low-relief surfaces, spatial and temporal exhumation patterns, and river profile morphologies matching observations on the SE Tibetan Plateau.

Beyond the SE Tibetan Plateau, our modeling may help explain the formation of high-elevation, low-relief surfaces in the southern Pyrenees (Babault et al., 2005; Bosch et al., 2018), the Andes (Kennan et al., 1997; Barke and Lamb, 2006), and the Himalayas (van der Beek et al., 2009; Adams et al., 2016). Progressive, unidirectional uplift in an outward propagating sequence is likely to occur in these mountain ranges because crustal thickening promotes the formation of a tectonic ramp at the range margin, with high rock uplift rates that propagate outward and advance the range front during shortening (e.g., Jammes and Huismans, 2012; Wolf et al., 2021). Such crustal ramps and outward propagating uplift have been inferred in the southern Pyrenees (Muñoz, 1992), the Andes (Armijo et al., 2009), and the Himalayan-Tibetan orogen (Wang et al., 2014; Li et al., 2015). Our modeling shows that this pattern of propagating uplift generates high-elevation, low-relief surfaces in tectonically active mountain belts, implying potential preservation of tectonic signals in mountain topography.

ACKNOWLEDGMENTS

The work is part of the COLORS project funded by TOTAL. We thank Huiping Zhang, who provides the data of low-relief surfaces. We thank Marin Clark, Benjamin Gérard, and an anonymous reviewer for their constructive comments.

References

Adams, B.A., Whipple, K.X., Hodges, K.V. and Heimsath, A.M., 2016. In situ development of high-elevation, low-relief landscapes via duplex deformation in the Eastern Himalayan hinterland, Bhutan. Journal of Geophysical Research: Earth Surface, 121(2), 294-319.

Armijo, R., Lacassin, R., Coudurier-Curveur, A. and Carrizo, D., 2015. Coupled tectonic evolution of Andean orogeny and global climate. Earth-Science Reviews, 143, 1-35.

Babault, J., Van Den Driessche, J., Bonnet, S., Castelltort, S. and Crave, A., 2005. Origin of the highly elevated Pyrenean peneplain. Tectonics, 24(2), doi:10.1029/2004TC001697.

Barke, R. and Lamb, S., 2006. Late Cenozoic uplift of the Eastern Cordillera, Bolivian Andes. Earth and Planetary Science Letters, 249(3-4), 350-367.

Bosch, G.V., Van Den Driessche, J., Babault, J., Robert, A., Carballo, A., Le Carlier, C., Loget, N., Prognon, C., Wyns, R. and Baudin, T., 2016. Peneplanation and lithosphere dynamics in the Pyrenees. Comptes Rendus Géoscience, 348(3-4), 194-202.

Clark, M.K. and Royden, L.H., 2000. Topographic ooze: Building the eastern margin of Tibet by lower crustal flow. Geology, 28(8), 703-706.

Clark, M. K., House, M. A., Royden, L. H., Whipple, K. X., Burchfiel, B. C., Zhang, X., Tang, W., 2005. Late Cenozoic uplift of southeastern Tibet. Geology, 33(6), 525-528.

Clark, M.K., Royden, L.H., Whipple, K.X., Burchfiel, B.C., Zhang, X., Tang, W., 2006. Use of a regional, relict landscape to measure vertical deformation of the eastern Tibetan Plateau. Journal of Geophysical Research: Earth Surface, 111(F03002), doi:10.1029/2005JF000294.

Epis, R. and Chapin, C.E., 1975. Surface in the Southern Rocky Mountains. In Cenozoic History of the Southern Rocky Mountains: Papers Deriving from a Symposium Presented at the Rocky Mountain Section Meeting of the Geological Society of America, Boulder, Colorado (Vol. 144). Geological Society of America.

Fox, M. and Carter, A., 2020. How continuous are the “Relict” landscapes of Southeastern Tibet? Frontiers in Earth Science, 8, doi:10.3389/feart.2020.587597.

Henck, A.C., Huntington, K.W., Stone, J.O., Montgomery, D.R. and Hallet, B., 2011. Spatial controls on erosion in the Three Rivers Region, southeastern Tibet and southwestern China. Earth and Planetary Science Letters, 303(1-2), 71-83.

Jammes, S. and Huismans, R.S., 2012. Structural styles of mountain building: Controls of lithospheric rheologic stratification and extensional inheritance. Journal of Geophysical Research: Solid Earth, 117(B10), doi:10.1029/2012JB009376.

Kennan, L., Lamb, S.H. and Hoke, L., 1997. High-altitude palaeosurfaces in the Bolivian Andes: evidence for late Cenozoic surface uplift. Geological Society, London, Special Publications, 120(1), 307-323.

Li, H.A., Dai, J.G., Xu, S.Y., Liu, B.R., Han, X., Wang, Y.N. and Wang, C.S., 2019. The formation and expansion of the eastern Proto-Tibetan Plateau: Insights from low-temperature thermochronology. Journal of Asian Earth Sciences, 183, https://doi.org/10.1016/j.jseaes.2019.103975

Li, Y., Wang, C., Dai, J., Xu, G., Hou, Y. and Li, X., 2015. Propagation of the deformation and growth of the Tibetan–Himalayan orogen: A review. Earth-Science Reviews, 143, 36-61.

Liu-Zeng, J., Zhang, J., McPhillips, D., Reiners, P., Wang, W., Pik, R., Zeng, L., Hoke, G., Xie, K., Xiao, P. and Zheng, D., 2018. Multiple episodes of fast exhumation since Cretaceous in southeast Tibet, revealed by low-temperature thermochronology. Earth and Planetary Science Letters, 490, 62-76.

Muñoz, J.A., 1992. Evolution of a continental collision belt: ECORS-Pyrenees crustal balanced cross-section. In Thrust tectonics (pp. 235-246). Springer, Dordrecht.

Ouimet, W., Whipple, K.X., Royden, L.H., and Granger, D., 2005. Long transient response times of rivers in eastern Tibet to regional plateau uplift: The effect of mega-landslides, Geophys. Res. Abstr., 7, Abstract 05743.

Ouimet, W., Whipple, K., Royden, L., Reiners, P., Hodges, K., Pringle, M., 2010. Regional incision of the eastern margin of the Tibetan Plateau. Lithosphere, 2(1), 50-63.

Perron, J.T., Royden, L., 2013. An integral approach to bedrock river profile analysis. Earth Surface Processes and Landforms, 38(6), 570-576.

Sinclair, H., 2017. Making a mountain out of a plateau. Nature, 542(7639), 41-42.

Schoenbohm, L.M., Burchfiel, B.C. and Liangzhong, C., 2006. Propagation of surface uplift, lower crustal flow, and Cenozoic tectonics of the southeast margin of the Tibetan Plateau. Geology, 34(10), 813-816.

Tian, Y., Kohn, B.P., Gleadow, A.J. and Hu, S., 2014. A thermochronological perspective on the morphotectonic evolution of the southeastern Tibetan Plateau. Journal of Geophysical Research: Solid Earth, 119(1), 676-698.

van Der Beek, P., Van Melle, J., Guillot, S., Pêcher, A., Reiners, P.W., Nicolescu, S. and Latif, M., 2009. Eocene Tibetan plateau remnants preserved in the northwest Himalaya. Nature Geoscience, 2(5), 364-368.

Wang, C., Dai, J., Zhao, X., Li, Y., Graham, S.A., He, D., Ran, B. and Meng, J., 2014. Outward-growth of the Tibetan Plateau during the Cenozoic: A review. Tectonophysics, 621, 1-43.

Whipple, K.X., 2001. Fluvial landscape response time: how plausible is steady-state denudation? American Journal of Science, 301(4-5), 313-325.

Whipple, K.X., DiBiase, R.A., Ouimet, W.B. and Forte, A.M., 2017. Preservation or piracy: Diagnosing low-relief, high-elevation surface formation mechanisms. Geology, 45(1), 91-94.

Wobus, C., Whipple, K.X., Kirby, E., Snyder, N., Johnson, J., Spyropolou, K., Crosby, B., Sheehan, D. and Willett, S.D., 2006. Tectonics from topography: Procedures, promise, and pitfalls. Special Papers-Geological Society of America, 398, 55-74.

Wolf, S. G., Huismans, R. S., Muñoz, J.-A., Curry, M. E., and van der Beek, P. (2021). Growth of collisional orogens from small and cold to large and hot— inferences from geodynamic models. Journal of Geophysical Research: Solid Earth, 126, e2020JB021168

Yang, R., Willett, S.D. and Goren, L., 2015. In situ low-relief landscape formation as a result of river network disruption. Nature, 520(7548), 526-529.

Yuan, X.P., Braun, J., Guerit, L., Rouby, D., Cordonnier, G., 2019. A new efficient method to solve the stream power law model taking into account sediment deposition. Journal of Geophysical Research: Earth Surface, 124, 1346-1365.

Figure 1. The study area in the Tibetan Plateau. A, Map of the Tibetan Plateau. **B**, Closer view of the study area with the high-elevation, low-relief surfaces on the SE Tibetan Plateau. Black curves show the catchment boundaries of the Salween, Mekong and Yangtze Rivers. Trunk channels of the Three Rivers are colored with the channel steepness k_{sn} from Equation 1 (see text for details). Yellow shading shows low-relief surfaces as identified in Clark et al. (2006). **C**, χ-elevation plot (Equation DR7) using *m*/*n* = 0.4 (yellow: Salween; green: Mekong; magenta: Yangtze) (see text for details). The same data for a range of values of m/n are shown in Fig. DR2. **D-F**, Mainstem river profiles, the maximum and mean topography of 20-km wide swaths parallel to rivers with mean annual precipitation.

Figure 2. Landscape evolution model of the SE Tibetan Plateau in response to southeastward propagating uplift and horizontal shortening using FastScape (Yuan et al., 2019). **A**, River network and elevation shown at 50 Ma, 25 Ma, and 0 Ma (Movie DR1). A cross section of rock uplift rate U (mm/yr) is plotted below the panels. **B**, Channel steepness k_{sn} ($m^{0.8}$) in Equation 1 (Movie DR2). **C**, χ values using Equation DR7 and the low-relief surfaces (yellow shading areas) with surface slope <4° (Movie DR3). The modeled low-relief surfaces exist in the headwaters and interfluves above deep valley, consistent with observations (Fig. 1B). Box area shows the modeled χ-elevation plots of interior and exterior rivers in Fig. DR6A. **D**, The river profile at 0 Ma and maximum elevation in a 150-km wide swath profile, as well as erosion rate (blue) along the river profile. Black and colored dots show several representative locations of landscape in **A**. **E**, Topography at 30 Ma, 15 Ma, and 0 Ma located at the dashed lines in **A**.

Figure 3. Spatial and temporal exhumation patterns and χ-elevation comparisons for two modeled uplift scenarios. **A**, Total exhumation over 50 Myr of modeled landscape evolution using the propagating uplift scenario, with black and colored dots showing the locations of exhumation histories displayed in **B**. The cyan and orange dots are situated on low-relief interfluves between deep valleys and headwaters, respectively. **C**, Comparison of modeled and observed χ-elevation plots for the mainstem rivers using the erodibility $K_f = 1.2 \times 10^{-6}$ $m^{0.2}/yr$. **D**, Total exhumation over 50 Myr of the uniform uplift scenario using the same erodibility, with black dots showing the locations of exhumation histories along the mainstem rivers in **E**. **F**, Comparison of modeled and observed χ-elevation plots for the mainstem rivers.

Figure 1

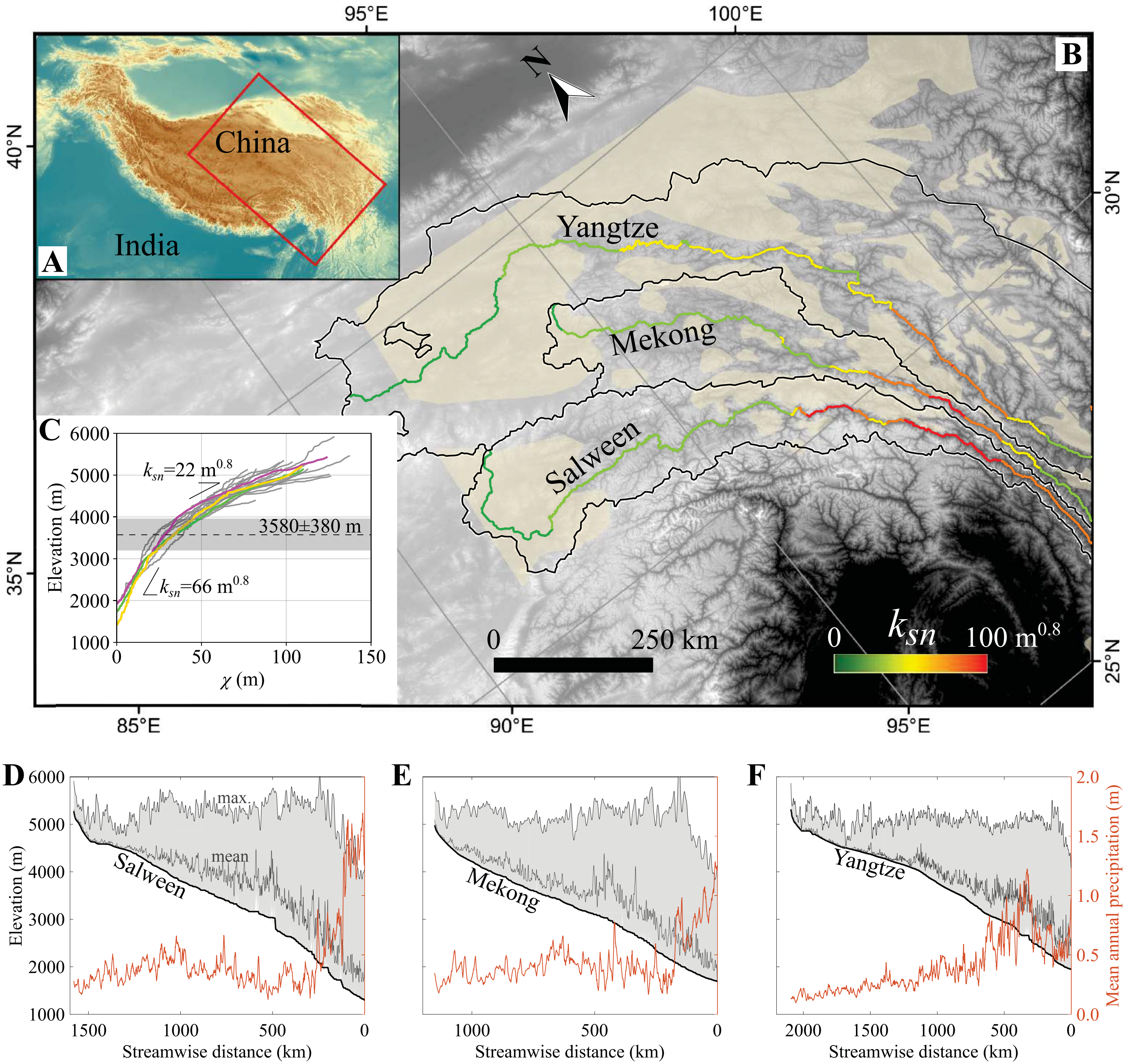

95°E
100°E
40°N
30°N
35°N
25°N
85°E
90°E
95°E
B
N
China
India
A
Yangtze
Mekong
Salween
C
k_{sn}=22 m$^{0.8}$
3580±380 m
k_{sn}=66 m$^{0.8}$
Elevation (m)
χ (m)
0
250 km
k_{sn}
0
100 m$^{0.8}$
D
E
F
max.
mean
Salween
Mekong
Yangtze
Elevation (m)
Streamwise distance (km)
Streamwise distance (km)
Streamwise distance (km)
Mean annual precipitation (m)

Figure 2

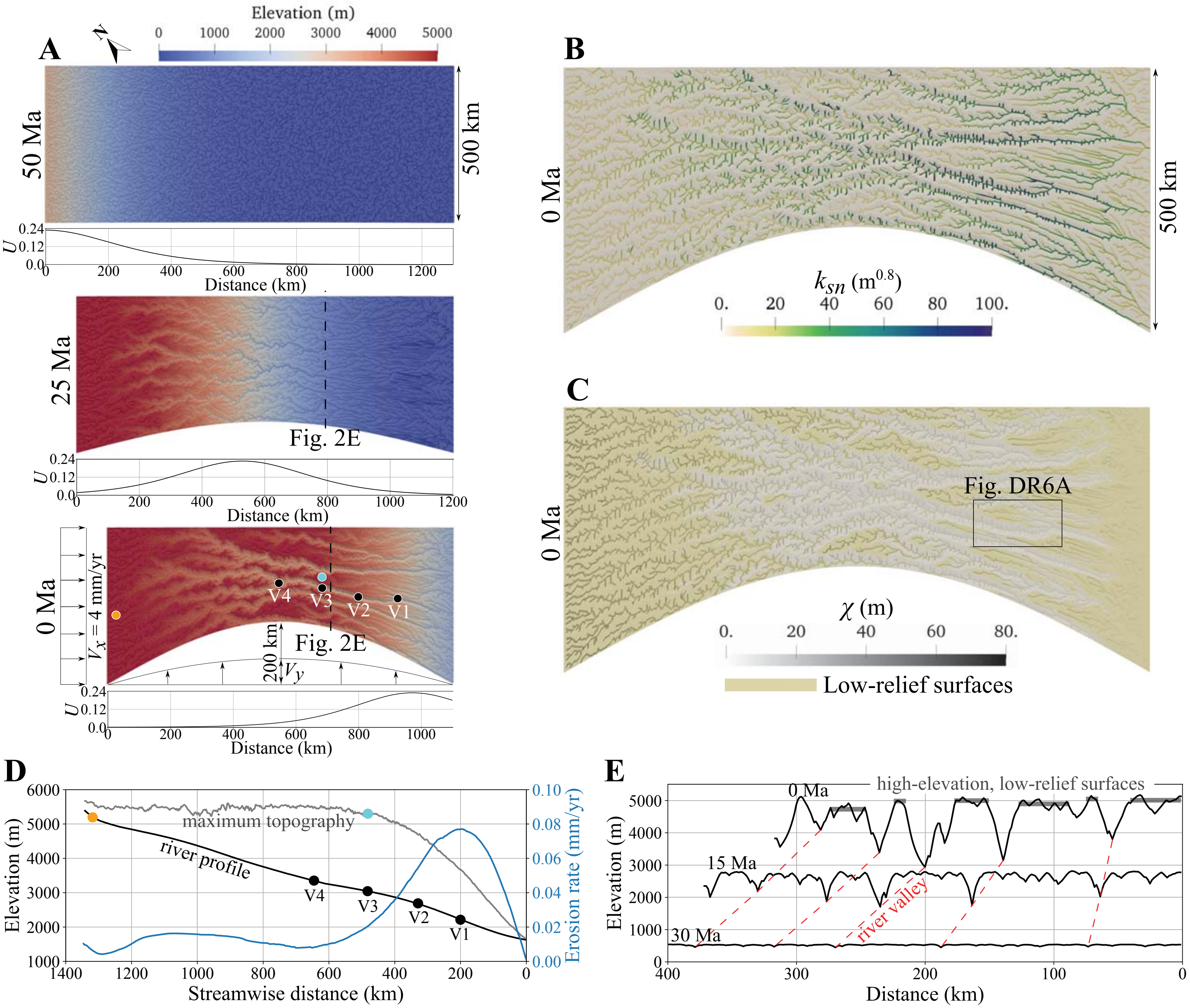

A
Elevation (m)
0
1000
2000
3000
4000
5000
N
50 Ma
500 km
U
Distance (km)
25 Ma
Fig. 2E
0 Ma
V_x = 4 mm/yr
V4
V3
V2
V1
200 km
V_y
B
k_{sn} ($m^{0.8}$)
C
Fig. DR6A
χ (m)
Low-relief surfaces
D
Elevation (m)
Erosion rate (mm/yr)
maximum topography
river profile
Streamwise distance (km)
E
high-elevation, low-relief surfaces
15 Ma
30 Ma
river valley
Distance (km)

Figure 3

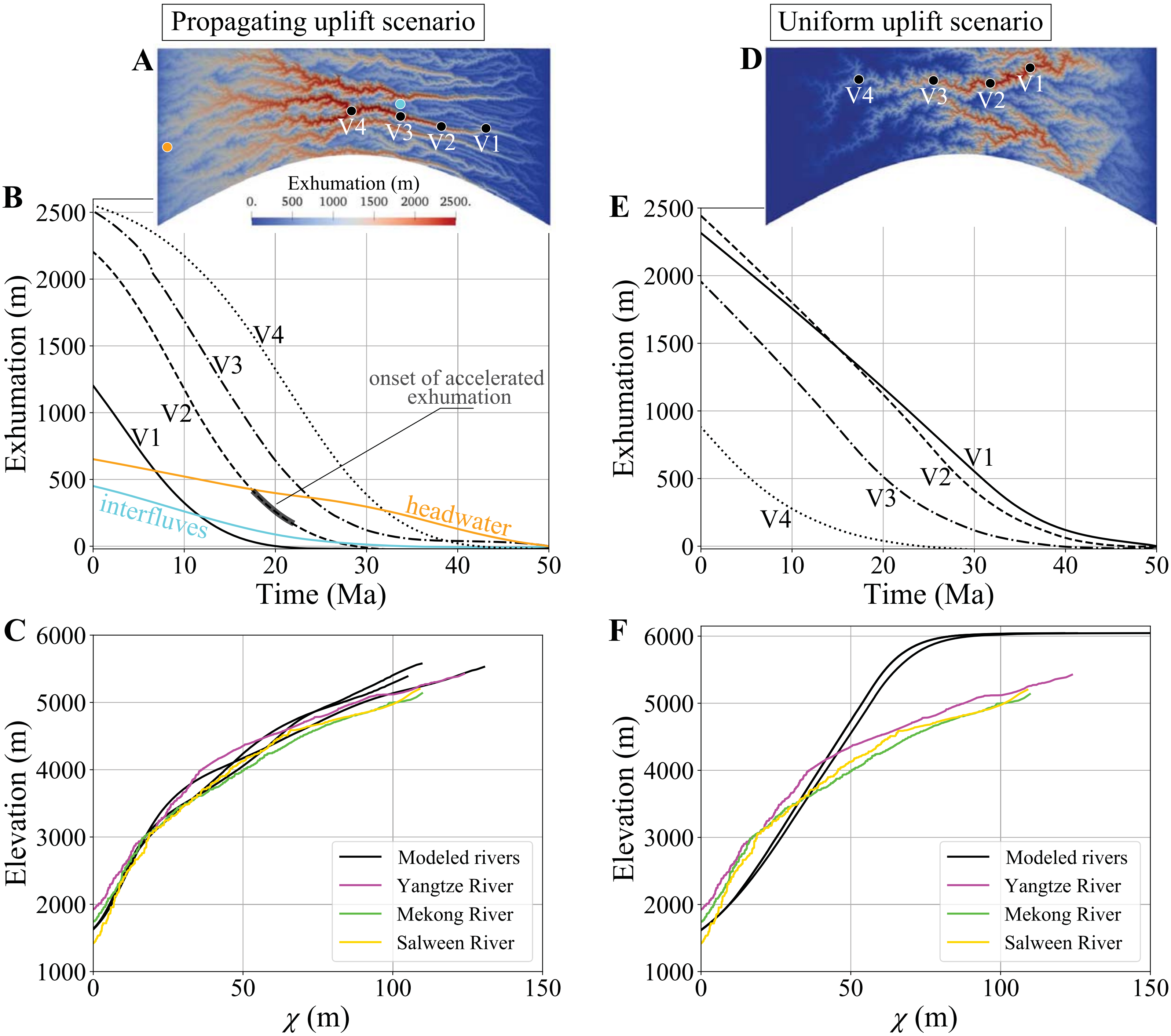

Propagating uplift scenario
Uniform uplift scenario
A
D
V1
V2
V3
V4
Exhumation (m)
0. 500 1000 1500 2000 2500.
B
E
Exhumation (m)
Time (Ma)
onset of accelerated exhumation
headwater
interfluves
C
F
Elevation (m)
χ (m)
Modeled rivers
Yangtze River
Mekong River
Salween River